

Effect of molecular architecture on the morphology diversity of the multi-compartment micelles: A dissipative particle dynamics simulation study

Ying Zhao, Ying-Tao Liu, Zhong-Yuan Lu*, Chia-Chung Sun

State Key Laboratory of Theoretical and Computational Chemistry, Institute of Theoretical Chemistry, Jilin University, Changchun 130023, China

ARTICLE INFO

Article history:

Received 31 May 2008

Received in revised form 30 July 2008

Accepted 27 August 2008

Available online 16 September 2008

Keywords:

Multicompartment micelles
Dissipative particle dynamics simulation
Molecular architecture

ABSTRACT

Dissipative particle dynamics simulation is performed to study the sensitive influence of the molecular architecture and/or segment sequence on the morphology diversity of the multicompartment micelles. The multicompartment micelle morphologies formed by ABC triblock copolymers with various molecular architectures, such as the linear, the pentalinear, the cyclic, the star-like, the tetra-arm, and the π -shape are investigated, and different morphologies of the multicompartment micelles, for example, worm-like, “hamburger”, sheet-like with pores, “sweet potato” with alternating layers, sheet-like with cylinder-inclusion, and three-dimensional network are observed in this work. The density profiles and the radial distribution functions are calculated to characterize the structures of the multicompartment micelles. The preparation of complex multicompartment micelles can be fulfilled by simply changing the segment sequence and molecular architecture such as adding new bonds and grafting points.

© 2008 Elsevier Ltd. All rights reserved.

1. Introduction

The self-assembly of multiblock copolymers into multi-compartment micelles had received increasing attentions in recent years, mainly due to their characterized structures of segregated incompatible subdomains and their wide applications, for example, in the drug delivery and nanotechnology [1–18]. The concept of multicompartment micelles, firstly proposed by Ringsdorf in the mid-1990s, drew inspiration from organized biological systems [8]. The multicompartment micelles are nanoscopic aggregates that possess a hydrophilic shell and one to several compartments in a hydrophobic core, which can perform an array of distinct functions. For example, in the nanobiotechnology, the separated incompatible compartments of the hydrophobic core could entrap and release various hydrophobic drugs selectively, while the hydrophilic shell would stabilize these nanostructures [8,9,12].

In these years, diverse strategies for preparing stable multi-compartment micelles in aqueous media had been developed by several groups [7–15]. Since the pioneer work by Lodge and co-workers [1], most investigations had been focused on the structure and morphology of multicompartment micelles formed from star triblock copolymers, which had stimulated the field of advanced colloidal systems. For example, Lodge and co-workers synthesized a series of ABC miktoarm star triblock copolymers in water containing a hydrocarbon, a fluorocarbon, and a hydrophilic block, and

observed various morphologies of multicompartment micelles such as worm-like, “hamburger”, raspberry, and sheet [1,3,4]. Laschewsky and co-workers found the “spheres on spheres” multicompartment micelles prepared by the self-assembly in aqueous medium of linear ABC triblock copolymers PVBM-*b*-PS-*b*-PVBFP [9]. Thünemann et al. observed two-sphere and cylindrical multicompartment micelles formed from linear ABCBA pentablock copolymer PEO-*b*-PBLG-*b*-PFPE-*b*-PBLG-*b*-PEO in dilute aqueous solution [10].

Much progress has been made on the preparation of the multi-compartment micelles, but experimental investigation is still not easy. The difficulties in the experiments limit the observations of the fine structures of the multicompartment micelles, especially the hydrophobic core. Moreover, a lot of factors, for example, the structure of the multiblock copolymer (including the chemical constitution, the relative lengths of the individual block, and the chain architecture) and the property of the solution (such as the concentration, the temperature, pH, and the specific solvent) can influence the morphology and structure of the nanoscopic aggregates, which must be explored in a wide parameter space, taking a huge number of experimental effort [20,21]. Therefore, molecular simulation technique, as a time and cost efficient tool, can not only complement experimental works with a wide parameter space, but also give a preview of phenomena prior to experiments [21–35].

Recently, dissipative particle dynamics (DPD) simulation technique had been illustrated to be a powerful tool for better understanding the self-assembly mechanism of the multicompartment micelles [21]. For example, Zhong and co-workers using DPD not only identified new morphologies by varying block lengths, block

* Corresponding author.

E-mail address: luzhy@mail.jlu.edu.cn (Z.-Y. Lu).

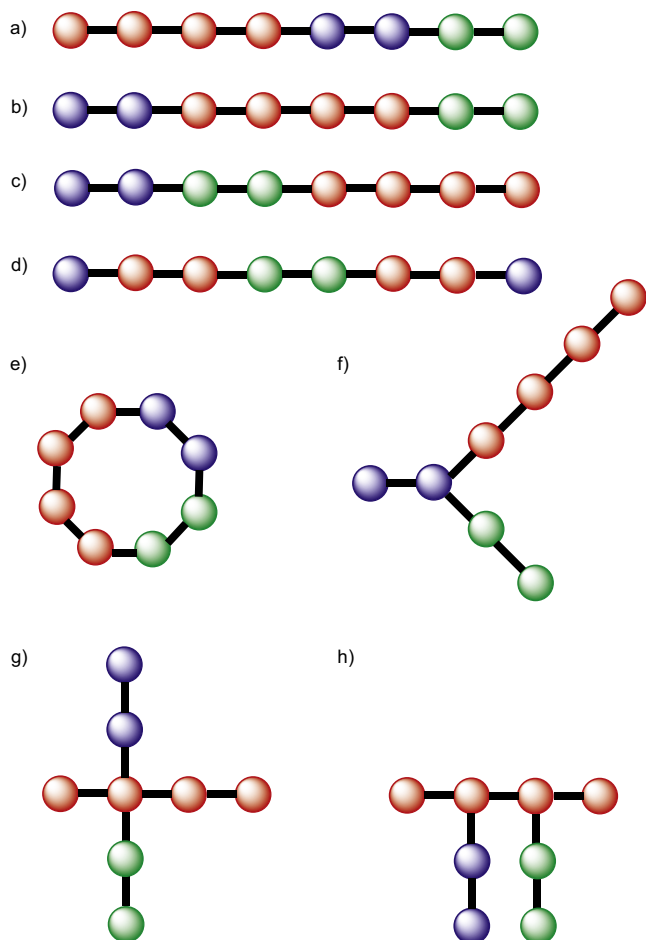


Fig. 1. Schematic structures for the eight model block copolymers: (a): $A_4B_2C_2$ (linear1) linear triblock copolymer; (b): $B_2A_4C_2$ (linear2) linear triblock copolymer; (c): $B_2C_2A_4$ (linear3) linear triblock copolymer; (d): $BA_2C_2A_2B$ linear pentablock copolymer; (e): $A_4B_2C_2$ cyclic triblock copolymer; (f): $B_2A_4C_2$ star-like triblock copolymer; (g): $A_4B_2C_2$ tetra-arm triblock copolymer; (h): $A_4B_2C_2$ π -shape triblock copolymer.

ratios, and solvent qualities in a systematic way, but also studied the formation process of multicompartment micelles [21–25]. Chou et al. performed DPD simulations to study the effects of molecular architecture, block length, and solution concentration on the morphologies of ABC terpolymers [35]. However, the knowledge about the influence of the block copolymer architecture and/or segment sequence on the morphology of the multicompartment micelles is still very little. In any case, such information is very interesting for chemists, especially since well-controlled polymerization techniques (such as atom transfer radical polymerization, reversible addition fragmentation transfer polymerization, and nitroxide-mediated polymerization) are popular nowadays to synthesize block copolymers with diverse architectures [19].

In experiments, the simplest block copolymer that can form multicompartment micelles is the ABC type triblock copolymer. Thus in this work, we focus exclusively on the influence of the molecular architecture and the segment sequence of ABC triblock copolymers on the formation of the multicompartment micelles. The multicompartment micelle morphologies formed by ABC triblock copolymers with various molecular architectures, such as the linear, the cyclic, the star-like, the tetra-arm, and the π -shape (shown in Fig. 1), are studied with DPD simulations, in each of case, the block sizes of A, B, and C are kept constant. The structures of the multicompartment micelles are then characterized by the density profiles and the radial distribution functions.

2. Model and simulation details

The DPD method is a mesoscopic simulation technique introduced by Hoogerbrugge and Koelman in 1992 [36]. A DPD bead represents a group of atoms or a volume of fluid that is large on the atomistic scale but still macroscopically small [37]. The force experienced by particle i is composed of three parts: a conservative force F^C , a dissipative force F^D , and a random force F^R . To model the block copolymers, we tie the adjacent beads in a single polymer chain by harmonic spring force F^S . Each force is pairwise additive:

$$F_i = \sum_{j \neq i} (F_{ij}^C + F_{ij}^D + F_{ij}^R + F_{ij}^S). \quad (1)$$

The sum runs over all other particles within a certain cutoff radius r_c . The different parts of the forces are given by:

$$F_{ij}^C = -\alpha_{ij}\omega^C(r_{ij})e_{ij}, \quad (2)$$

$$F_{ij}^D = -\gamma\omega^D(r_{ij})(v_{ij} \cdot e_{ij})e_{ij}, \quad (3)$$

$$F_{ij}^R = \sigma\omega^R(r_{ij})\xi_{ij}\Delta t^{-1/2}e_{ij}, \quad (4)$$

$$F_{ij}^S = Cr_{ij}, \quad (5)$$

where $r_{ij} = r_i - r_j$, $r_{ij} = |r_{ij}|$, $e_{ij} = r_{ij}/r_{ij}$, and $v_{ij} = v_i - v_j$. ξ_{ij} is a random number with zero mean and unit variance, chosen independently for each interacting pair of particles at each time step Δt . α_{ij} is a constant which describes the maximum repulsion between interacting beads. The number density of our model is 3. The repulsion parameter is actually related to the Flory–Huggins χ -parameter by:

$$\alpha_{ij} \approx \alpha_{ii} + 3.27\chi_{ij} \quad (\rho = 3), \quad (6)$$

where the interaction parameter between the same bead type α_{ii} equals 25 to correctly describe the compressibility of water [37]. ω^C , ω^D , and ω^R are three weight functions for the conservative, dissipative and random forces, respectively. For the conservative force, we choose $\omega^C(r_{ij}) = 1 - r_{ij}$ for $r_{ij} < 1$ and $\omega^C(r_{ij}) = 0$ for $r_{ij} \geq 1$. $\omega^D(r_{ij})$ and $\omega^R(r_{ij})$ have a certain relation according to the fluctuation-dissipation theorem [38],

$$\omega^D(r) = [\omega^R(r)]^2, \quad \sigma^2 = 2\gamma k_B T. \quad (7)$$

Here we choose a simple form of ω^D and ω^R following Groot and Warren [37],

$$\omega^D(r) = [\omega^R(r)]^2 = \begin{cases} (1-r)^2 & (r < 1) \\ 0 & (r \geq 1) \end{cases} \quad (8)$$

The parameter C is set to be 4.0, which is enough to keep the adjacent beads connected together along the polymer backbone [39].

A modified version of velocity–Verlet algorithm [37,39] (Groot–Warren integrator) is used here to integrate the equations of motion according to Ref. [37]. For easy numerical handling, we have chosen the cutoff radius, the particle mass, and the temperature as the unit of the simulated system, i.e., $r_c = m = k_B T = 1$. As a consequence, the unit of time τ is $\tau = r_c \sqrt{m/k_B T} = 1$.

Although DPD is a simple but intrinsically promising simulation method to study the multicompartment micelles, computational cost is still a limiting factor. Our DPD code is thus parallelized using

Table 1
DPD bead-bead interaction parameters α_{ij}

	W	A	B	C
W	25	50	27	120
A	50	25	45	75
B	27	45	25	90
C	120	75	90	25

a spatial domain decomposition method [40,41] with the aid of the standard message passing interface library. To validate our DPD code, we first simulate the self-assembly of star block copolymer $A_4B_8C_2$ into multicompartment micelles and the “worm-like” micelles are observed which is consistent with those of Refs. [7,22].

In literatures, Zhong and co-workers had determined [22] the DPD repulsion parameters between unlike species of ABC block copolymers based on the famous experimental work of Lodge and co-workers [1], in which the star triblock copolymers consisted of the weakly hydrophobic polyethylene (denoted as A), the hydrophilic poly(ethylene oxide) (denoted as B), and the strongly hydrophobic poly(perfluoropropylene oxide) (denoted as C). For the best comparison between our results with those from literatures and experiments, in this work, we just adopt the DPD repulsion parameters according to Ref. [22] as shown in Table 1. The water molecule (W) is modeled as a single DPD bead, and the triblock copolymers $A_4B_2C_2$ are modeled by connected DPD beads. It should be noted that different types of block copolymers possess the same chemical composition but different molecular architecture and segment sequence. The simulations are performed in a cubic cell of size $32 \times 32 \times 32r_c^3$ containing 9.8304×10^4 DPD beads. To validate the correctness of obtained morphologies of the multicompartment micelles, 1.92×10^5 DPD beads in $40 \times 40 \times 40r_c^3$ cubic box are simulated for the systems of the star-like, the tetra-arm and the π -shaped triblock copolymers. The volume fraction of the triblock copolymers is 0.10 to guarantee the dilute aqueous solution. Other concentrations are not included in this study. Periodic boundary conditions are applied. The time step Δt is taken as 0.05, $2\text{--}5 \times 10^5$ DPD time steps are carried out to attain equilibration for each system.

3. Results and discussion

3.1. Effects of the segment sequence of the linear triblock copolymer

The linear triblock copolymers with different segment sequences such as ABC, ACB, and BAC can self-assemble into various morphologies which possess different potential applications [9,43–48]. To illustrate the influence by simply changing the segment

sequence along the block copolymer backbone while keeping the chain length and the chemical composition unvaried, we study the self-assembly process and structures from linear $A_4B_2C_2$ (denoted as linear1), $B_2A_4C_2$ (linear2), and $B_2C_2A_4$ (linear3) triblock copolymers via DPD simulations. The typical morphologies of the obtained multicompartment micelles are shown in Fig. 2: (a) worm-like cylindrical micelle for linear1, (b) oblate “hamburger” with block C core for linear2, and (c) oblate “hamburger” with block A core for linear3. The equilibrium self-assembly of micelles is dominated by free energy change. However, in our cases, the chain is comparatively short and the repulsion between different blocks is strong. Thus the obtained multicompartment morphologies are mainly controlled by the competitive interactions between different bead-pairs, especially by the interactions between the beads of block copolymer and water. In solution, weakly hydrophilic B should protect strongly hydrophobic C from contacting to the solvent. Although the three linear triblock copolymers possess identical chemical composition, their self-assembly morphologies are totally different. It clearly reflects the sensitive dependence of the multicompartment micelle structure on the segment sequence. For linear1, B connects to A and C, it cannot protect C effectively; therefore the worm-like multicompartment micelle with alternating A, B, and C compartments is found. For linear2, B connects to A then to C; therefore a hamburger-like micelle with core C and shell B layered by A is found. For linear3, B connects to C then to A; therefore a hamburger-like micelle with core A and shell B layered by C is found. In the latter two cases, the linear triblock copolymer can be taken as a weakly hydrophilic part (block B) connected with a hydrophobic part (block A and C), thus they possess similar micelle structure (hamburger-like) but with different cores. The shape of the micelle is also determined by the free energy. The ideal micelle morphology should be spherical with C surrounded by A then by B, which contacts to water solely. But the weakly hydrophilic part is always shorter than the hydrophobic parts for our triblock copolymers, thus the typical spherical micelle structure with longer hydrophilic chains cannot appear. The micelles prefer the maximum (minimum) contacting between B (C) and water, meanwhile to avoid the free energy penalty due to drastic interface curvature change. These complex factors, together with, for example, the interfacial energy between the regions of different blocks, determine the equilibrium micelle structures [1,44].

The density profiles (ρ) of the A, B, and C components in different directions are calculated in order to better describe the morphologies of the multicompartment micelles (Fig. 3a–c). For example, from Fig. 3a which shows the density profiles along Y direction, we find alternating maxima of components A, B, and C, which reflect the layer by layer structure of the multicompartment micelle formed by linear1 ($A_4B_2C_2$). From Fig. 3b we can find an enrichment region of C

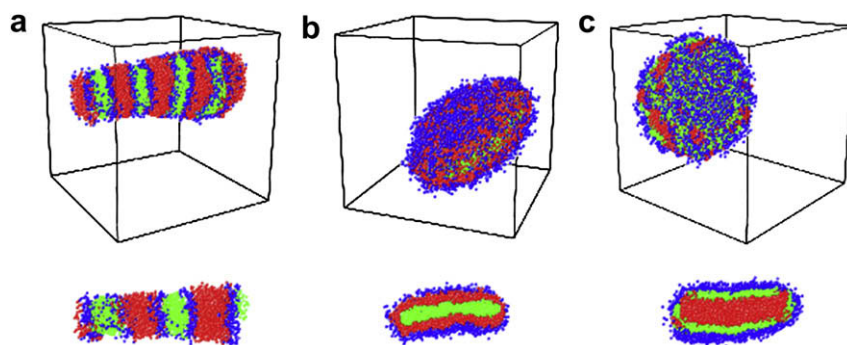


Fig. 2. Morphologies of the multicompartment micelles of (a): $A_4B_2C_2$ linear1 triblock copolymer; (b): $B_2A_4C_2$ linear2 triblock copolymer; (c): $B_2C_2A_4$ linear3 triblock copolymer. Water beads are omitted. Block A, red; block B, blue; and block C, green. The positions of the multicompartment micelles are shifted to appear in the box center (roughly) for clarity. The crosssections below the morphologies are also shown to demonstrate the fine structures of the micelles. (For interpretation of the references to colour in this figure legend, the reader is referred to the web version of this article.)

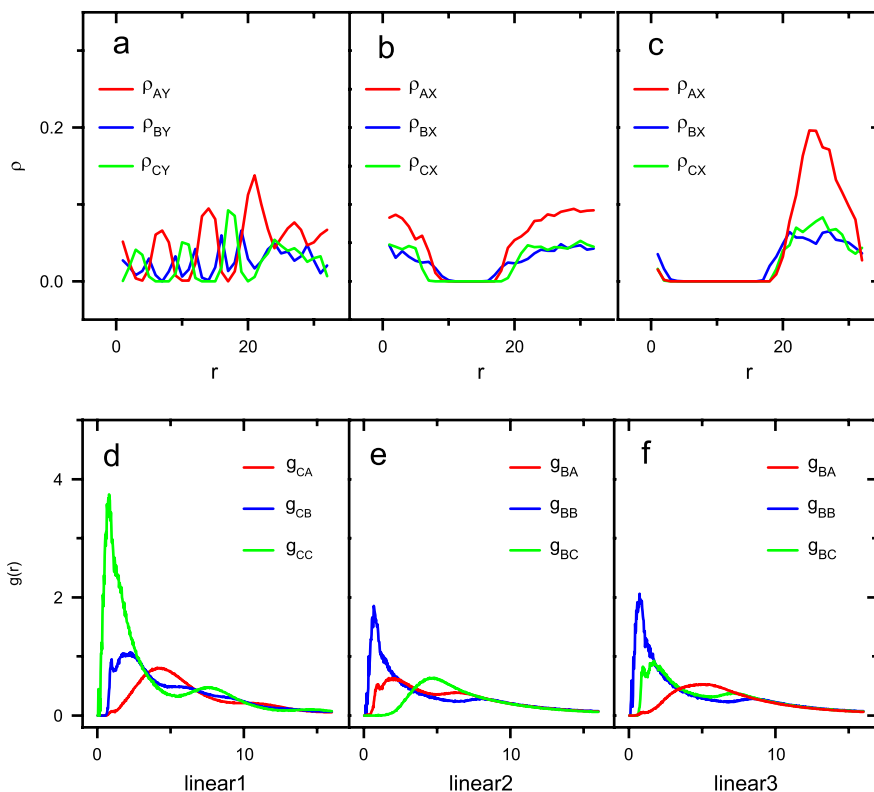


Fig. 3. The density profiles in X or Y direction are shown for (a): $A_4B_2C_2$ linear1 triblock copolymer; (b): $B_2A_4C_2$ linear2 triblock copolymer; (c): $B_2C_2A_4$ linear3 triblock copolymer. The radial distribution functions are shown for (d): $A_4B_2C_2$ linear1 triblock copolymer; (e): $B_2A_4C_2$ linear2 triblock copolymer; (f): $B_2C_2A_4$ linear3 triblock copolymer. Block A, red; block B, blue; block C, green. (For interpretation of the references to colour in this figure legend, the reader is referred to the web version of this article.)

indicated by the maximum of the green line, which corresponds to the core region of the “hamburger” micelle structure of linear2 ($B_2A_4C_2$) as shown in Fig. 2b. Similarly, from Fig. 3c we can find an enrichment region of A indicated by the maximum of the red line, which corresponds to the core region of the “hamburger” micelle structure of linear3 ($B_2C_2A_4$) as shown in Fig. 2c.

The radial distribution functions $g(r)$ are also calculated to analyze the structures of the multicompartment micelles. The function gives the probability of finding a pair of particles with a distance r apart, which is formally defined by [49]

$$g(r) = \frac{V}{N^2} \left\langle \sum_i \sum_{j \neq i} \delta(r - r_{ij}) \right\rangle, \quad (9)$$

where N is the number of particles and V is the volume of the simulation box. $g(r)$ between A, B, and C components of linear1, linear2, and linear3 triblock copolymers are calculated and shown in Fig. 3d–f, respectively. Fig. 3d corresponds to $g(r)$ of the multicompartment micelle formed by linear1 triblock copolymer. Although the second peak is flat, there are apparently two peaks for $g_{CC}(r)$, which reflect the typical layered structure. $g_{CC}(r)$ possesses the highest peak as shown in Fig. 3d, which can be attributed to the compact aggregation formed by C block. Moreover, the position at which $g(r)$ shows maximum is in the order $r_{CC} < r_{CB} < r_{CA}$, as shown in Fig. 3d. This implies the layer sequence and spacing in the segmented worm-like structure of the multicompartment micelle formed by linear1. Fig. 3e corresponds to $g(r)$ of the micelle formed by linear2 triblock copolymer. No two-peak characteristics appear in $g(r)$; thus the micelle does not possess periodic layered structure. From Fig. 3e, we can find that the aggregates of C are near to A but far from B. In combination with the fact that block B is weakly hydrophilic and blocks A and C are hydrophobic, a “hamburger” micelle structure with block C as the core can be easily deduced.

Similarly, from Fig. 3f, we can find that the aggregate A is near to C and far from B. Thus a “hamburger” micelle structure with block A as the core can be deduced.

The sequence of the domain is the same as that of the block along the chain backbone for linear1, which is due to the short chain length of hydrophilic block B. One can imagine if block B is longer, linear1 may not self-assemble into a worm-like micelle structure with domain B distributed in between domains A and C. Block B should stretch into the solution and protect the hydrophobic core formed by A and C. We thus have studied the self-assembly of linear1 system with a series of block B lengths at the same simulation conditions. With increasing block B length, the micelle is no longer worm-like, instead it looks like a network of long tubes.

3.2. Effects of the topology confinement of the triblock copolymer

The multicompartment micelles formed by triblock copolymers with various topological structures were extensively investigated [1–4,7,12,21,24,25,35]. The influence of the molecule topology on the block copolymer self-assembly morphologies can be mainly ascribed to the chemical confinement effect such as new bonds and grafting points. For example, by connecting the ends of linear triblock copolymer $A_4B_2C_2$, we obtain a cyclic triblock copolymer $c - A_4B_2C_2$ with no free ends. By cutting different bonds between components A, B, and C of $c - A_4B_2C_2$, the linear1, linear2, and linear3 triblock copolymers will be formed. In this section, we will study the molecule topology effects of triblock copolymers on the multicompartment micelle morphologies.

3.2.1. The comparison between linear triblock $B_2A_4C_2$ (linear2) and pentablock $BA_2C_2A_2B$ copolymers

It is now possible to prepare the multicompartment micelles by self-assembly of linear pentablock copolymers in experiments

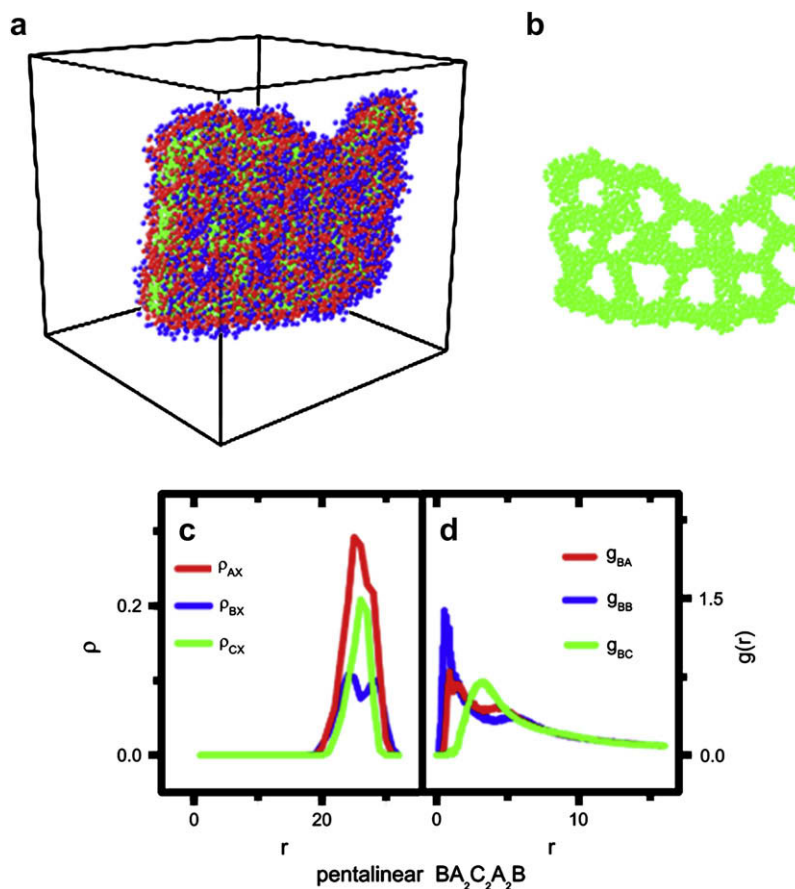


Fig. 4. (a) and (b): Morphology of the multicompartment micelle, (c): the density profiles in X direction and (d): the radial distribution function of $BA_2C_2A_2B$ linear pentablock copolymer. Block A, red; block B, blue; block C, green. (For interpretation of the references to colour in this figure legend, the reader is referred to the web version of this article.)

[10,52]. Recently, computer simulations were also successfully applied to study the multicompartment micelle structures formed by linear pentablock copolymers [23,50,51]. In this subsection we will compare the micelle morphology difference of linear triblock $B_2A_4C_2$ and pentablock $BA_2C_2A_2B$ copolymers.

Simply connecting the end beads of the C blocks from different linear $B_2A_4C_2$ triblock copolymers will form a linear pentablock copolymer $B_2A_4C_4A_4B_2$. This pentablock copolymer possesses the same chemical composition as the triblock copolymer but with twice the chain length. To make the comparison at the same chain length, we thus consider the pentablock copolymer $BA_2C_2A_2B$ which not only has the same chain length as the linear triblock copolymers, but also possesses the same chemical sequence along the chain backbone as $B_2A_4C_4A_4B_2$. This pentablock copolymer, $BA_2C_2A_2B$, is symmetric; it is formed by connecting the C beads of different BA_2C , which is the linear triblock copolymer by dividing each block size of $B_2A_4C_2$ by 2. Comparing $BA_2C_2A_2B$ with $B_2A_4C_2$, we can find that the results of the pentablock copolymer $BA_2C_2A_2B$ self-assembly can also reflect the effect of varying segment sequences. It is of course possible to generate a lot of different segment sequences for a pentablock copolymer by playing mathematics based on a chemical composition, but we do not try to do so since the number of possible combination is actually unlimited. It should be noted that, in this research, we focus on the effects of segment sequence and the molecular architecture on the morphology diversity of the multicompartment micelles exclusively. Thus other influence factors such as the concentration and the chain length are not systematically considered.

Fig. 4a shows the self-assembly micelle morphology of pentablock copolymer $BA_2C_2A_2B$. Interestingly, a sheet-like flat micelle with porous C domains in the core is found, which is similar to that

obtained by Liu and Zhong in Ref. [23]. Now the question is what is the reason that this special micelle structure emerges. First of all, we need to check if it is the result of topology confinement effect. Therefore, we obtain the equilibrium self-assembly morphology of pentablock copolymer $B_2A_4C_4A_4B_2$ via DPD simulation at the same condition. The resulted multicompartment micelle formed by $B_2A_4C_4A_4B_2$ is hamburger-like, which is very similar to that of linear triblock copolymer $B_2A_4C_2$. It implies that the topology confinement by adding a new bond between two triblock copolymers to form a symmetric linear pentablock copolymer does not influence the self-assembly morphology if the chain length is long enough. Thus the emergence of sheet-like flat micelle with porous C domains in the core for $BA_2C_2A_2B$ must be due to other factors.

To characterize this sheet-like micelle structure clearly, we also calculate the density profiles and the radial distribution functions which are shown in Fig. 4c and d. From the density profiles we can see that the sheet is very thin in X direction (Fig. 4c). Moreover, we can directly compare $g(r)$ for $BA_2C_2A_2B$ (Fig. 4d) with that for the triblock copolymer $B_2A_4C_2$ (Fig. 3e). For both block copolymers, the B and C beads aggregate to form the shell and the core regions for a multicompartment micelle. Thus the peak position for $g_{BC}(r)$ can roughly reflect half of the thickness of the hamburger-like or the sheet-like micelle. For $BA_2C_2A_2B$ and $B_2A_4C_2$, we find half of the thicknesses are 3.3 and 4.8, respectively. The decrease of micelle thickness by changing $B_2A_4C_2$ to $BA_2C_2A_2B$ can partially explain why the sheet-like multicompartment micelle is continuous – the thinner micelle possesses larger area.

In Fig. 5, we show some typical snapshots during the self-assembly of linear $BA_2C_2A_2B$ in water. In the beginning of the simulation, a lot of small micelles with hamburger-like morphology are observed; then the nearby micelles merge to form larger

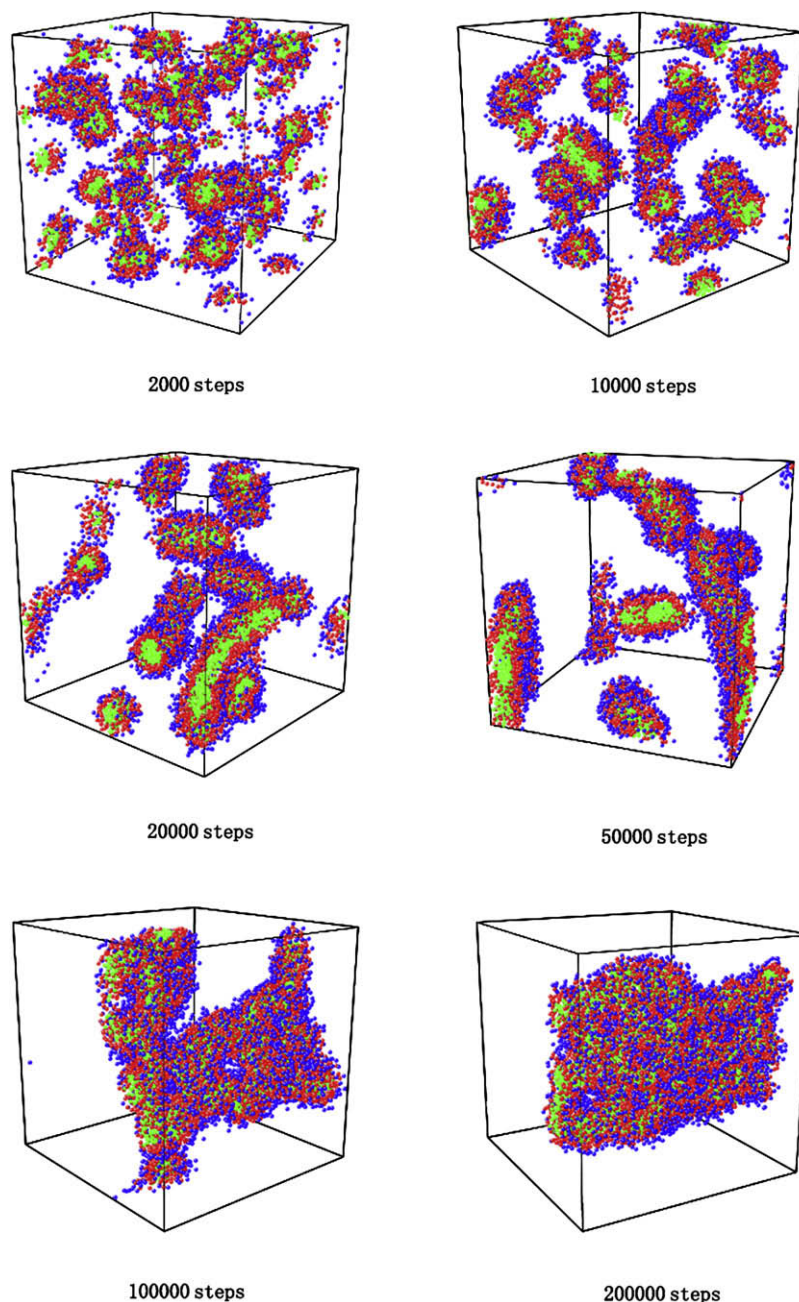


Fig. 5. Some typical snapshots during the self-assembly of linear $BA_2C_2A_2B$ in water.

micelles and long micelles. These micelles are all hamburger-like, with C as the core and B as the shell. After 1×10^5 time steps, the large micelles merge to form a continuous micelle which is very similar to the final morphology. Half of the symmetric pentablock copolymer $BA_2C_2A_2B$ is BA_2C , which is the triblock copolymer obtained by dividing each block of $B_2A_4C_2$ by two, thus the self-assembly morphology should be comparable between BA_2C and $B_2A_4C_2$. That is why we can always observe hamburger-like micelles during $BA_2C_2A_2B$ self-assembly. To some extents, the continuous sheet-like porous micelle of $BA_2C_2A_2B$ can also be taken as a special “hamburger”, which is flattened and perforated. Thus the morphologies formed by adding a new bond between two triblock copolymers, or in other words, with this topology confinement, are in essence the same to those of the linear2 triblock copolymer.

It is worthwhile to check if the periodic boundary conditions in the simulation help the formation of the sheet-like porous micelle. We

then study a solution of $BA_2C_2A_2B$ with all the simulation conditions unchanged except for the volume fraction of the block copolymer being 5%. This time we still find a porous micelle but it is isolated in the solution. Therefore, the natural self-assembly morphology of the multicompartment micelle formed by $BA_2C_2A_2B$ should be porous. Its emergence may not be due to the topology confinement effect (since for $B_2A_4C_4A_4B_2$ we have found a hamburger-like micelle), but instead simply due to too short B block lengths.

3.2.2. The comparison between the cyclic and the linear triblock copolymers

Chemically bonding two end particles of a linear triblock copolymer will result in a cyclic triblock copolymer which possesses no free ends. Another characteristics of this topology confinement are the hydrophilic block being connected to two hydrophobic blocks. The self-assembly morphology of the cyclic

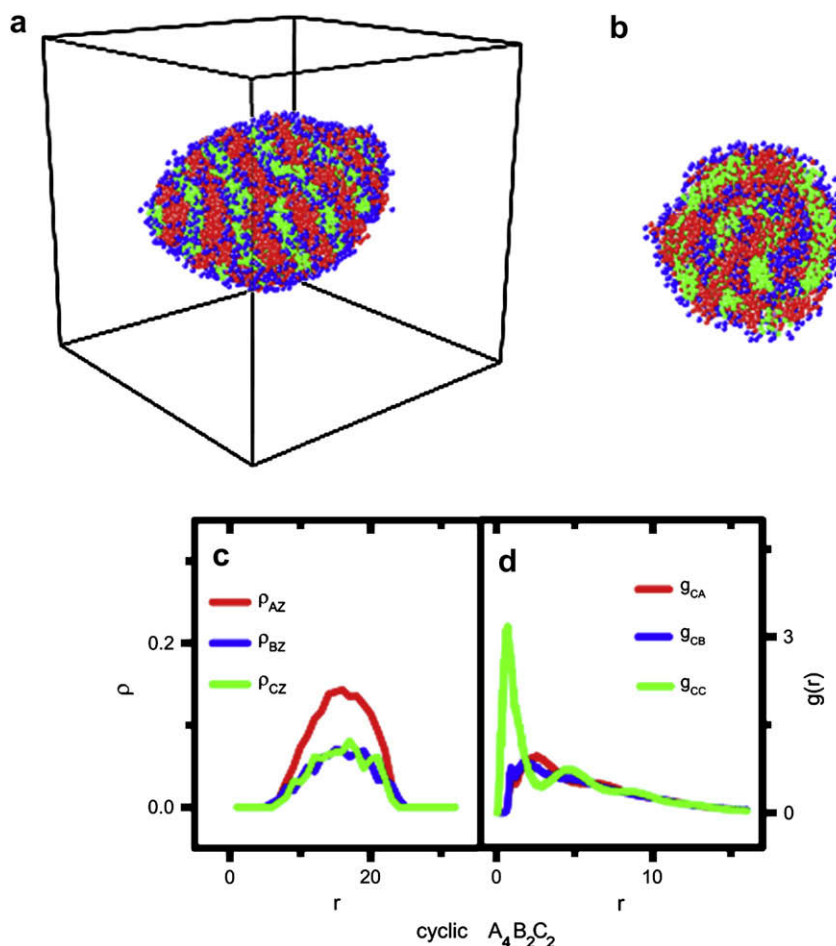


Fig. 6. (a) and (b): Morphology of the multicompartment micelle, (c): the density profiles in Z direction and (d): the radial distribution function of $A_4B_2C_2$ cyclic triblock copolymer. Block A, red; block B, blue; block C, green. (For interpretation of the references to colour in this figure legend, the reader is referred to the web version of this article.)

triblock copolymer $A_4B_2C_2$ in water is shown in Fig. 6a and b. The micelle looks like a sweet potato with alternating layers composed by A and C blocks. Most of the B particles distribute above block C to protect this strongly hydrophobic region. By viewing the cross-section of the micelle, we also find the layers (twisted and interconnected) which are composed by A, B, and C blocks.

The micelle morphology of the cyclic triblock copolymer $A_4B_2C_2$ can further be characterized by the density profiles and the radial distribution functions, as shown in Fig. 6c and d. The density fluctuation in Fig. 6c indicates the layered structure of the micelle; but this layered structure is twisted and not as good as that shown in Figs. 2a and 3a for linear $A_4B_2C_2$. Especially, the radial distribution function $g_{CC}(r)$ possesses two peaks, which reflect an alternating layered micelle structure with constant layer spacing (roughly). Thus the morphology of the multicompartment micelle formed by cyclic $A_4B_2C_2$ is similar to that formed by linear $A_4B_2C_2$. This is due to the structural similarity between cyclic $A_4B_2C_2$ and linear $A_4B_2C_2$: their hydrophilic blocks are always connected by two hydrophobic blocks. In comparison with the other two linear triblock copolymer models $B_2A_4C_2$ and $B_2C_2A_4$, the cyclic $A_4B_2C_2$ triblock copolymer does not possess free hydrophilic ends (B) which can extend in water to protect the hydrophobic cores (A and C), but instead, the hydrophilic blocks are forced to appear in between the hydrophobic regions formed by A and C. Thus the self-assembly morphology of cyclic $A_4B_2C_2$ has a layered structure, similar to that of linear $A_4B_2C_2$ and in contrast to the hamburger-like morphology formed by linear $B_2A_4C_2$ and $B_2C_2A_4$.

The results emphasize the strong influence of the topology confinement due to connecting the free hydrophilic ends on the

multicompartment micelles, as compared to the pentablock case which is topologically confined by connecting two hydrophobic ends.

3.2.3. Effects of the graft points

We have discussed the effects of the segment sequence and the topology confinement of the bonded chain ends on the multicompartment micelle morphologies. Other possible molecule topology variations can be resulted by the change of the graft points, which may also influence the micelle morphology via self-assembly. For example, for a constant chemical composition $A_4B_2C_2$ we can have different molecule topologies, such as star-like (Fig. 1f), tetra-arm (g), and π -shape (h). In the following, we will show the sensitive influence of the topology difference on the multicompartment micelle morphology.

The mean-square radius of gyration of star-like, tetra-arm, and π -shape triblock copolymer is much smaller than that of linear block copolymer [42]. Since smaller mean-square radius of gyration corresponds to smaller lateral domain size, the micelle structures of star-like, tetra-arm, and π -shape triblock copolymers are most likely extended. To avoid the artificial effects due to the periodic boundary conditions, we expand the system to $40 \times 40 \times 40r_c^3$ and keep other simulation conditions unchanged. The obtained equilibrium micelle morphologies are shown in Fig. 7a for star-like ABC triblock copolymer which is worm-like cylinder with defects, in (b) for tetra-arm ABC triblock copolymer which is sheet-like with cylinders formed by block C, and in (c) for π -shape ABC triblock copolymer which is a three-dimensional network.

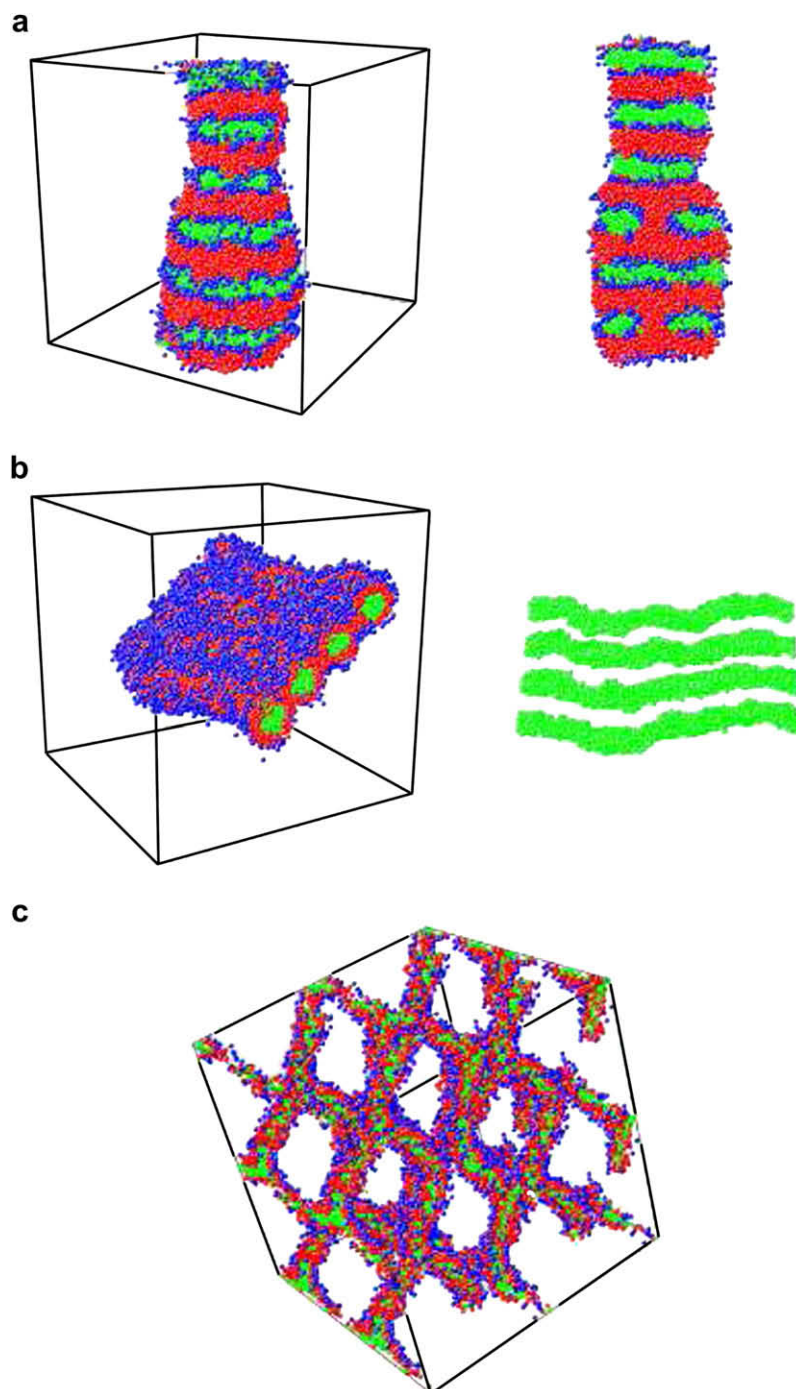


Fig. 7. Morphologies of the multicompartiment micelles of (a): $B_2A_4C_2$ star-like triblock copolymer; (b): $A_4B_2C_2$ tetra-arm triblock copolymer; (c): $A_4B_2C_2$ π -shape triblock copolymer. The water beads are omitted. Block A, red; block B, blue; and block C, green. The positions of the multicompartiment micelles are shifted to appear in the box center (roughly) for clarity. The cross sections below the morphologies are also shown to demonstrate the fine structures of the micelles. It should be noted that the simulation box is duplicated in X, Y, and Z directions to show the network structure of the micelle formed by $A_4B_2C_2$ π -shape triblock copolymer. (For interpretation of the references to colour in this figure legend, the reader is referred to the web version of this article.)

The morphologies can also be characterized by the particle density profiles in Z direction and the radial distribution functions between particle pairs. From Fig. 8a, the layer by layer worm-like structure of the micelle can be demonstrated by the density profile in Z direction, which shows an alternating density distributions of A, B, and C. However, the micelle defects (Fig. 7a) cannot be reflected in the density profiles. As shown in Fig. 8b, the densities for A, B, and C particles in Z direction show strong fluctuations in the aggregation region. These fluctuations actually imply periodic inner structures in Z direction of the micelle, as demonstrated in

Fig. 7b. However, the network structure for π -shape ABC triblock copolymer is hard to be distinguished by the density profiles as shown in Fig. 8c.

Fig. 8d–f shows the radial distribution functions, $g(r)$, between components A, B, and C for star-like, tetra-arm, and π -shape triblock copolymers. The multi-peaks in the curves of $g(r)$ as shown in Fig. 8d apparently imply the layer by layer structure of the multicompartiment micelle formed by star-like triblock copolymer. Fig. 8e characterizes the column-in-the-sheet structure of the multicompartiment micelle formed by tetra-arm triblock

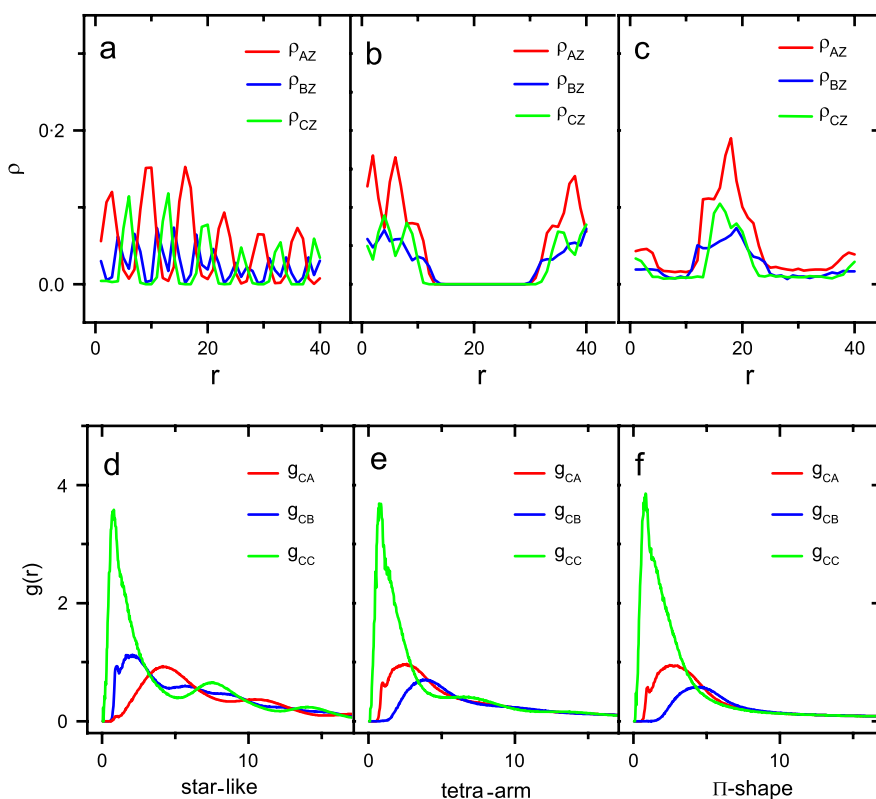


Fig. 8. The density profiles in Z direction are shown for (a): $B_2A_4C_2$ star-like triblock copolymer; (b): $A_4B_2C_2$ tetra-arm triblock copolymer; (c): $A_4B_2C_2$ π -shape triblock copolymer. The radial distribution functions are shown in (d): for $B_2A_4C_2$ star-like triblock copolymer; (e): $A_4B_2C_2$ tetra-arm triblock copolymer; (f): $A_4B_2C_2$ π -shape triblock copolymer. Block A, red; block B, blue; block C, green. (For interpretation of the references to colour in this figure legend, the reader is referred to the web version of this article.)

copolymer. The position at which $g(r)$ shows maximum is in the order $r_{CC} < r_{CA} < r_{CB}$. This reflects that the hydrophobic core is formed by block C which is surrounded by weakly hydrophobic block A, then by hydrophilic B. The shoulder peak as shown in $g_{CC}(r)$, though not clear, is the characteristics of the locally ordered arrangement of columns formed by block C as the micelle core. From Fig. 8f, we can easily find that domain order is C, A, and B from micelle core to the shell, consistent with that of the tetra-arm triblock copolymer, but the network structure can not be identified with the aid of $g(r)$.

The complex multicompartment micelle structures due to the molecule topology variations well illustrate the sensitive influence of the chemical constraint. The topology differences between the three triblock copolymers reside in that: star-like: one graft point, three branches; tetra-arm: one graft point, four branches; π -shape: two graft points, four branches. The graft points possess the smallest degree of freedom and must appear in the interfaces, which consequently change the free energy via spontaneous interfacial curvature. The star-like triblock copolymer as shown in Fig. 1f actually has very similar topology as that of linear1 (a). The only difference is that a B particle is removed from the chain backbone of linear1 and attached to the other B particle from the side chain to form this star-like triblock copolymer. Therefore, their self-assembly structures are nearly identical, both form cylindrical worm-like multicompartment micelles. Since for this star-like triblock copolymer, the B particle must appear in the A, B, and C interfaces, more defects are found in the equilibrium micelle morphology (as shown in Fig. 7a). It should be noted that the star-like topology of the triblock copolymer does not correspond to only one molecule structure as shown in Fig. 1f, but also other triblock copolymer structures are possible, for example, those structures as shown in Fig. 9a and d. Their self-assembly morphologies are obtained in the simulations and shown in Fig. 9b, c, and e. The

molecule structure as shown in Fig. 9a is that three A particles are removed from the chain backbone of linear2 and attached to the other A particle from the side chain. The corresponding micelle morphology as shown in Fig. 9b is inter-connected tubes formed by C, surrounded by B then by A, which is not similar to that of linear2 because of long A block length in the side chain. The molecule structure as shown in Fig. 9d is similar to linear3, so that its self-assembly morphology (e) is similar to that shown in Fig. 2c.

The tetra-arm triblock copolymer as shown in Fig. 1g is similar to the molecule structure of star-like triblock copolymer as shown in Fig. 9a, except that the B arm and the C arm are connected to the second A bead along the A arm. Therefore their self-assembly micelle morphologies are similar. It is interesting to find the influence of the branch point position: By changing the branch point from the end of A arm to the second bead of the A arm, the multicompartment micelle changes from a sweet potato-like (Fig. 9b) to a continuous sheet structure with separated C domains (Fig. 7b). By further moving the branch point of B or C arm of the $A_4B_2C_2$ tetra-arm triblock copolymer towards the other end of arm A, we can obtain the π -shape triblock copolymer, as shown in Fig. 1h. In this case we find that its self-assembly morphology is a three-dimensional network. It implies that the solution undergoes a sol-gel transition at this or even lower concentration. The inner structure of the network is also special, with C domains being surrounded by A then by B. Such a structure may help the development of the new hierarchically ordered oxides in experiments [53]. These results have clearly demonstrated the sensitive influence of the molecular architecture on the morphology of the multicompartment micelles of block copolymers. By slightly changing the number of branch points or the branch point positions, we have obtained diverse micelle structures which possess different application possibilities.

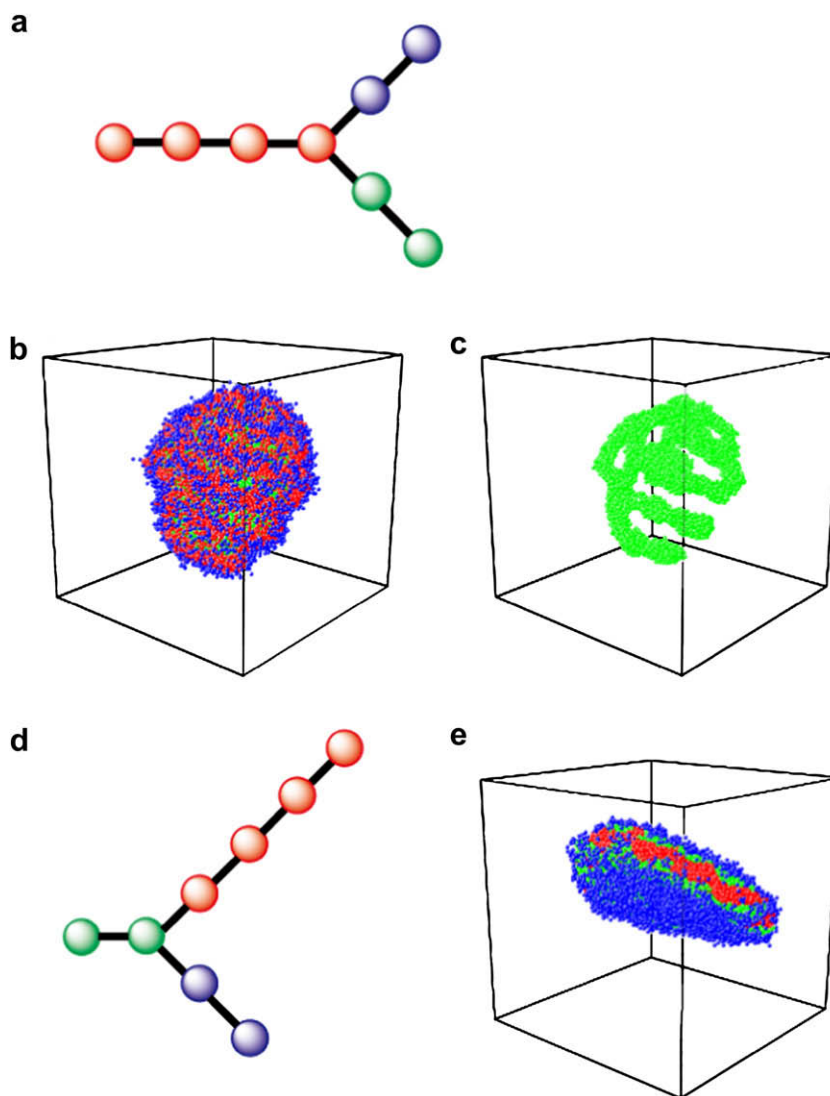


Fig. 9. (a), (b), and (c): The star-like triblock copolymer with B_2 and C_2 being connected to the end of A block; (d) and (e): the star-like triblock copolymer with B_2 and A_4 being connected to the end of C block. A bead: red; B bead: blue; C bead: green. (For interpretation of the references to colour in this figure legend, the reader is referred to the web version of this article.)

It should be noted that, for larger block copolymers, much more complex molecule structures exist, thus we can expect even novel micelle morphologies via the self-assembly of these molecules. As shown in this research, DPD simulations can serve as an ideal tool to help the design of the block copolymer structures and the corresponding micelle morphologies.

4. Conclusions

In this work, the sensitive influence of the segment sequence and the molecular architecture on the morphology diversity of the multicompartment micelles is investigated via dissipative particle dynamics, by simply changing the segment sequence along the linear triblock copolymer backbone and the molecular architecture such as adding new bonds and grafting points. Various multicompartment micelles are observed in our simulations. The structures of the multicompartment micelles are analyzed by the calculated density profiles and the radial distribution functions.

Since in our simulations, such a simple triblock copolymer $A_4B_2C_2$ with different segment sequence and/or the molecular architecture can form various multicompartment micelles, we believe that the morphologies of the multicompartment micelles

from the triblock copolymers with longer chain lengths are inevitably more complicated. The results in this work primarily complement the experiments with the possibilities on the preparation of the multicompartment micelles by changing the segment sequence and/or the molecular architecture of the triblock copolymers.

Acknowledgment

This work is supported by National Science Foundation of China (20490220, 20774036), and Fok Ying Tung Education Foundation (114018).

References

- [1] Li Z, Kesselman E, Talmon Y, Hillmyer MA, Lodge TP. *Science* 2004;306:98.
- [2] Li Z, Hillmyer MA, Lodge TP. *Macromolecules* 2006;39:765.
- [3] Li Z, Hillmyer MA, Lodge TP. *Nano Lett* 2006;6:1245.
- [4] Li Z, Hillmyer MA, Lodge TP. *Langmuir* 2006;22:9409.
- [5] Lodge TP, Rasdal A, Li Z, Hillmyer MA. *J Am Chem Soc* 2005;127:17608.
- [6] Zhou Z, Li Z, Ren Y, Hillmyer MA, Lodge TP. *J Am Chem Soc* 2003;125:10182.
- [7] Li Z, Hillmyer MA, Lodge TP. *Macromolecules* 2004;37:8933.
- [8] Laschewsky A. *Curr Opin Colloid Interface Sci* 2003;8:274.
- [9] Kubowicz S, Baussard JF, Lutz JF, Thünemann AF, Berlepsch Hv, Laschewsky A. *Angew Chem Int Ed* 2005;44:5262.

- [10] Thünemann AF, Kubowicz S, Berlepsch Hv, Möhwald H. *Langmuir* 2006;22:2506.
- [11] Kubowicz S, Thünemann AF, Weberskirch R, Möhwald H. *Langmuir* 2005;21:7214.
- [12] Lutz JF, Laschewsky A. *Macromol Chem Phys* 2005;206:813.
- [13] Stähler K, Selb J, Candau F. *Langmuir* 1999;15:7565.
- [14] Weberskirch R, Preuschen J, Spiess HW, Nuyken O. *Macromol Chem Phys* 2000;201:995.
- [15] Kotzev A, Laschewsky A, Adriaensens P, Gelan J. *Macromolecules* 2002;35:1091.
- [16] Matsuoka K, Moroi Y. *Curr Opin Colloid Interface Sci* 2003;8:227.
- [17] Stähler K, Selb J, Candau F. *Mater Sci Eng C* 1999;10:171.
- [18] Kujawa P, Raju BB, Winnik FM. *Langmuir* 2005;21:10046.
- [19] Lutz JF. *Polym Int* 2006;55:979.
- [20] Kita-Tokarczyk K, Grumelard J, Haefele T, Meier W. *Polymer* 2005;46:3540.
- [21] Zhong C, Liu D. *Macromol Theory Simul* 2007;16:141.
- [22] Xia J, Zhong C. *Macromol Rapid Commun* 2006;27:1110.
- [23] Liu D, Zhong C. *Macromol Rapid Commun* 2007;28:292.
- [24] Xia J, Liu D, Zhong C. *Phys Chem Chem Phys* 2007;9:5267.
- [25] Xia J, Zhong C. *Chin J Chem* 2007;25:1732.
- [26] Liu D, Zhong C. *Polymer* 2008;49:1407.
- [27] He YD, Qian HJ, Lu ZY, Li ZS. *Polymer* 2007;48:3601.
- [28] Huang CI, Fang HK, Lin CH. *Phys Rev E* 2008;77: 031804.
- [29] Huang CI, Yu HT. *Polymer* 2007;48:4537.
- [30] Huang CI, Hsueh HY, Lan YK, Lin YC. *Macromol Theory Simul* 2007;16:77.
- [31] Huang CI, Chiou YJ, Lan YK. *Polymer* 2007;48:877.
- [32] Kou DZ, Liang HJ. *J Phys Chem B* 2006;110:23557.
- [33] Huang R, Jiang Y, Liang HJ. *Chem Phys Chem* 2006;7:1950.
- [34] Jiang Y, Zhu JT, Jiang W, Liang HJ. *J Phys Chem B* 2005;109:21549.
- [35] Chou SH, Tsao HK, Sheng YJ. *J Chem Phys* 2006;125:194903.
- [36] Hoogerbrugge PJ, Koelman JMVA. *Europhys Lett* 1992;19:155.
- [37] Groot RD, Warren PB. *J Chem Phys* 1997;107:4423.
- [38] Español P, Warren PB. *Europhys Lett* 1995;30:191.
- [39] Groot RD, Madden TJ. *J Chem Phys* 1998;108:8713.
- [40] Boryczko K, Dzwiniel W, Yuen DA. *Concurrency Computat Pract Exper* 2002;14:137.
- [41] Sims JS, Martys N. *J Res Natl Inst Stand Technol* 2004;109:267.
- [42] Zimm BH, Stockmayer WH. *J Chem Phys* 1949;17:1301.
- [43] Bailey TS, Hardy CM, Epps III TH, Bates FS. *Macromolecules* 2002;35:7007.
- [44] Goldacker T, Abetz V, Stadler R, Erukhimovich I, Leibler L. *Nature* 1999;398:137.
- [45] Balsamo V, Gil G, Urbina de Navarro C, Hamley IW, von Gyldenfeldt F, Abetz V, et al. *Macromolecules* 2003;36:4515.
- [46] Zhu J, Jiang W. *Macromolecules* 2005;38:9315.
- [47] Schacher F, Walther A, Ruppel M, Müller AHE. *Polym Mater Sci Eng* 2007;96:94.
- [48] Sun M, Wang P, Qiu F, Tang P, Zhang H, Yang Y. *Phys Rev E* 2008;77: 016701.
- [49] Allen MP, Tildesley DJ. *Computer simulation of liquids*. Oxford: Clarendon Press; 1987.
- [50] Chushak Y, Travesset A. *J Chem Phys* 2005;123:234905.
- [51] Anderson JA, Travesset A. *Macromolecules* 2006;39:5143.
- [52] Determan MD, Guo L, Thiyagarajan P, Mallapragada SK. *Langmuir* 2006;22:1469.
- [53] Yang P, Deng T, Zhao D, Feng P, Pine D, Chmelka BF, et al. *Science* 1998;282:2244.